Two-stage Looped-tube Thermoacoustic Cooler – Design and Preliminary Testing

Samir Gh. YAHYA, Xiaoan MAO and Artur J. JAWORSKI

Abstract — **Design options for a travelling wave thermoacoustic refrigerator have been considered with the view of using it for thermal management of various enclosures/compartments. Acoustic drivers such as loudspeakers or linear motors are essential for such thermoacoustic devices as they enable the conversion of electrical to acoustic power. The theoretical knowledge of how to couple an acoustic driver to thermoacoustic refrigerators or engines efficiently has been illustrated by studying the performance of an acoustic driver when connected to selected types of acoustic networks. A final design comprising a two-stage refrigerator (two thermoacoustic cores in series) driven by two acoustic drivers (model 1S132, available from Q-Drive) has been presented. The experimental setup and instrumentation have been explained. Finally, preliminary characterization of the prototype has been performed.**

Keywords – **Acoustic driver's performance, Thermoacoustic refrigeration, Two-stage cooler.**

I. INTRODUCTION

THE interaction between heat and sound is known as thermoacoustic effect. Here thermal power can be converted to acoustic power propagating through a gas and vice versa [1, 2, 3 and 4]. Thermoacoustics is a relatively new technology with promising future potential due a number of advantages [5]. For instance, the lack of mechanical moving parts leads to high reliability and low maintenance. Similarly, the working gas is usually an inert gas which makes thermoacoustic devices environmentally friendly due to the absence of the ozone depleting chemicals. This research aims at creating a demonstrator of thermoacoustic refrigerator that could be further developed into a means of thermal management of various enclosures. The challenges in this research are three-fold: to meet the required acoustic condition for the driver available to the project, to provide the required cooling power and fit the resulting device comfortably within a given enclosure.

The four main components of a travelling wave thermoacoustic refrigerator are the acoustic driver, regenerator, heat exchangers and the resonator. Refrigeration relies on applying work to a system to transfer heat from the cold side of the system (cold reservoir or heat exchanger) to the hot side [3]. Therefore, acoustic drivers (loudspeakers, linear motors), are some of the most important components due to their function of converting electricity to mechanical (acoustic) power and thus providing the input work to the system. The working gas compresses and expands periodically when subjected to an acoustic wave, while the gas parcels move back and forth in the direction of the acoustic wave propagation. Compression and expansion, and associated changes in temperature, in the vicinity of a solid body (heat exchanger, regenerator) lead to localized heat transfer processes, while the gas displacement enables heat pumping processes leading to generation of the temperature gradient along the thermoacoustic core. The regenerators are porous structures with the hydraulic radius of pores much smaller than the thermal penetration depth. This is to ensure a good thermal contact between gas and solid to obtain a reversible thermodynamic process. Regenerators are typically built in the form of stacked layers of stainless steel woven mesh sandwiched between two heat exchangers (e.g. "cold" and "ambient") to communicate thermally with the surroundings.

The design of travelling wave thermoacoustic refrigerators has been a subject of several studies. Some of these have focused on constructing travelling wave thermoacoustic refrigerators that derive their acoustic power from travelling wave thermoacoustic engines [6, 7 and 8]. Others focus on using acoustic drivers, especially linear motors, due to their high power availability [9, 10 and 11], in order to drive the refrigeration. These consume electricity to deliver an acoustic power that can reach up to 8 kW with 80% efficiency. For such acoustic power levels, thermoacoustic refrigerators can achieve a significant cooling power. However, most of refrigerators constructed so far still show relatively low efficiency and cooling power.

The parameters of the four major components of a traveling wave thermoacoustic refrigerator such as their locations, cross-sectional area and lengths have been discussed and illustrated in publications by other thermoacoustic researchers [9, 10 and 11]. The preliminary design of the current travelling wave thermoacoustic refrigerator was derived from these publications and subsequently modified and optimized according to the needs of the current study [12]. Although there are some available articles regarding electro-dynamic drivers [13, 14 and 15], significant design challenges remain due to the lack of publications concerning the coupling of an acoustic driver to the rest of the acoustic network at a specific acoustic condition in order to operate efficiently in terms of impedance matching.

The main focus of this study is the design and test of a two-stage travelling wave thermoacoustic refrigerator – this choice having been made on account of its higher efficiency than a standing wave counterpart [16, 6 and 17]. The second focus of this study is the performance analysis of the coupled acoustic driver in terms of electrical to acoustic power conversion. The numerical DeltaEC modelling is compared to the results obtained from the laboratory prototype.

II. ACOUSTIC DRIVER ANALYSIS

A schematic diagram of an acoustic driver's piston with relevant acoustic conditions is shown in Figure 1. An acoustic driver provides an acoustic power at a given electrical power. The conversion from electrical power to acoustic power (acoustic driver performance or efficiency) depends on the acoustic conditions, such as pressure difference, volume flow rate and their relative phases across the piston, but also on the parameters of an acoustic driver itself. Both of these contribute to the performance of the driver.
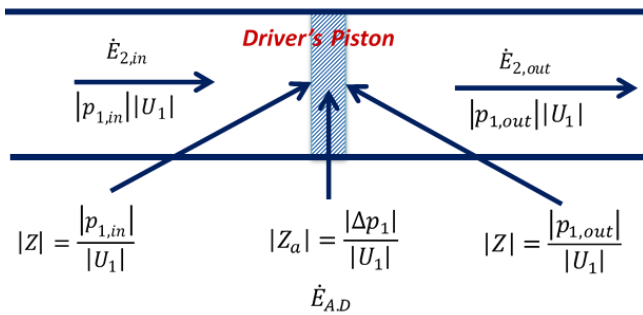

Figure 1. Acoustic driver condition around the piston of the acoustic driver.

Once the acoustic driver is fabricated, some of the parameters will be constant such as piston's diameter (D), coil electrical resistance (R_e), mechanical resistance (R_m), coil electrical inductance (L), BLProd, moving mass (M) and spring constant (K). Other parameters such as operating frequency (f) and oscillating voltage amplitude $(|V_1|)$ are the operating parameters which can be chosen within a limited range of an acoustic driver. Finally, any acoustic driver would have maximum or limited values of the peak to peak displacement of the piston $|2\xi_1|$, oscillating current amplitude $(|I_1|)$, acoustic power $(\dot{E}_2)$ and electrical power $(\dot{W}_e)$. It is strongly recommended to avoid these limitations during operation.

The acoustic power at the back, front and produced by the acoustic driver's piston can be theoretically calculated from Eq. (1, 2 and 3) respectively [3].

$$\dot{E}_{2,in} = \frac{1}{2}|p_{1,in}||U_1| \cos \Theta_{(p_{1,in} \& U_1)} \tag{1}$$

$$\dot{E}_{2,out} = \frac{1}{2}|p_{1,out}||U_1| \cos \Theta_{(p_{1,out} \& U_1)} \tag{2}$$

$$\dot{E}_{2,A.D} = \frac{1}{2}|\Delta p_1||U_1| \cos \Theta_{(\Delta p_1 \& U_1)}$$
$$or \quad \dot{E}_{2,A.D} = \dot{E}_{2,out} - \dot{E}_{2,in} \tag{3}$$

However, Eq. (2) can be used to estimate the produced acoustic power of the acoustic driver when the input acoustic power to driver ($\dot{E}_{2,in}$) and the pressure difference

across the piston ($|\Delta p_1|$) are either zero or negligible. The amplitude volume flow rate ($|U_1| = |\xi_1|\omega A_{A.D}$) of the acoustic driver can be calculated if the acoustic driver piston's diameter (D), operating frequency (f), $(\omega = 2\pi f)$ and the peak to peak displacement of the piston $|2\xi_1|$ are determined.

The consumed electrical power by the acoustic driver can be calculated from the following equation:

$$\dot{W}_e = \frac{1}{2}|I_1||V_1| \cos \Theta_{(I_1 \& V_1)} \tag{5}$$

If the complex values (real and imaginary values) of each; pressure difference $|\Delta p_1|$, volume flow rate $|U_1|$, given voltage $|V_1|$, consumed current $|I_1|$ and their relative phases are known then the produced acoustic power $\dot{E}_{2,A.D}$ and consumed electrical power $\dot{W}_e$ by the acoustic driver can be theoretically determined. Hence, the efficiency of the acoustic driver can be calculated via the following equation:

$$\eta_{A.D} = \frac{\dot{E}_{2,A.D}}{\dot{W}_e} \tag{6}$$

As mentioned earlier, the performance of an acoustic driver depends on the acoustic condition on both sides of the piston such as the amplitude and phase of the acoustic impedance. The performance of acoustic driver (1s132M by Q-Drive) has been analytically studied by utilizing the related equations when connected to an acoustic system at different acoustic impedance [12]. The acoustic impedance across the piston has been given a set of values between 10-100 Mpa.s/m³. The phase of the pressure difference has been set to be 0° while the phase of the volume flow rate changes from -90° to 90°. In other words, the phase of the acoustic impedance has been set to be between 90° to -90°, so the pressure difference can lead or lag the volume flow rate, as shown in Figure 2. To generate these graphs the operating frequency and peak to peak displacement of the piston have been set to 60 Hz and 12 mm, respectively. Further studies of the driver have been accomplished by setting the acoustic power to be 200 W and changing the frequency and peak to peak displacement, respectively. The limitations of the driver are 5.6 A, 140 V, 220 W of acoustic power and 350 W of electrical power.

Notably, the graphs show that when the acoustic impedance is above 70 Mpa.s/m3 and the phase is between -60° and -70° (i.e. volume flow rate leads the pressure difference by 60° to 70°), the acoustic driver achieves the maximum efficiency within the permitted current, voltage and acoustic and electrical power. Unfortunately, given the kind of acoustic networks used in this project it is apparent that the high impedance required by the alternator available would be difficult to provide. As a first step towards a closer match, a twin configuration of drivers is used to effectively double the produced acoustic power of a resulting twin driver. However, a further analysis and corrective measures in the network design have been described step by step in previous study [12].

III. EXPERIMENTAL APPARATUS AND INSTRUMENTATION

As it can be seen from Figure 3, the experimental apparatus consists of two cylindrical housing to accommodate the acoustic drivers (1S132M and 1S132DX). A compliance with a reducer have been used to connect the front of both acoustic drivers to an inertance. Both inertance and compliance have be utilized to deliver the preferable acoustic impedance of the acoustic drivers to work safely

and efficiently. The inertance is connected to the acoustic drivers from one end and a two-stage traveling-wave thermoacoustic cooler from the other end via a reducer and expander respectively. The two-stage traveling-wave thermoacoustic cooler consists of a torus tube and two identical thermoacoustic cores (see Table I). Each thermoacoustic core/stage has two identical heat exchangers (ambient and cold heat exchangers) and one regenerator made out of stainless steel and packed with stainless steel woven mesh screen discs. Each mesh screen has a hydraulic radius of 33.4 μm, which makes the value of the ratio of the hydraulic radius (r_h) to the thermal penetration depth $(\delta_\kappa = (2K/(\rho c_p\,\omega))^{0.5})$ to be 0.21. The heat exchangers are made of copper blocks. Each heat exchanger has 10 flow channels for the helium side as a working gas and 12 flow channels for the water side to inject and reject heat at the cold and hot ends of the regenerator at the ambient temperature. The flow channels consist of a number of fins created by using E.D.M technology (Electrical discharge machining). The fin thickness is 0.5 mm, with 1mm gaps between the fins, which makes 22% of the total cross-sectional area open to the oscillating working gas (helium).
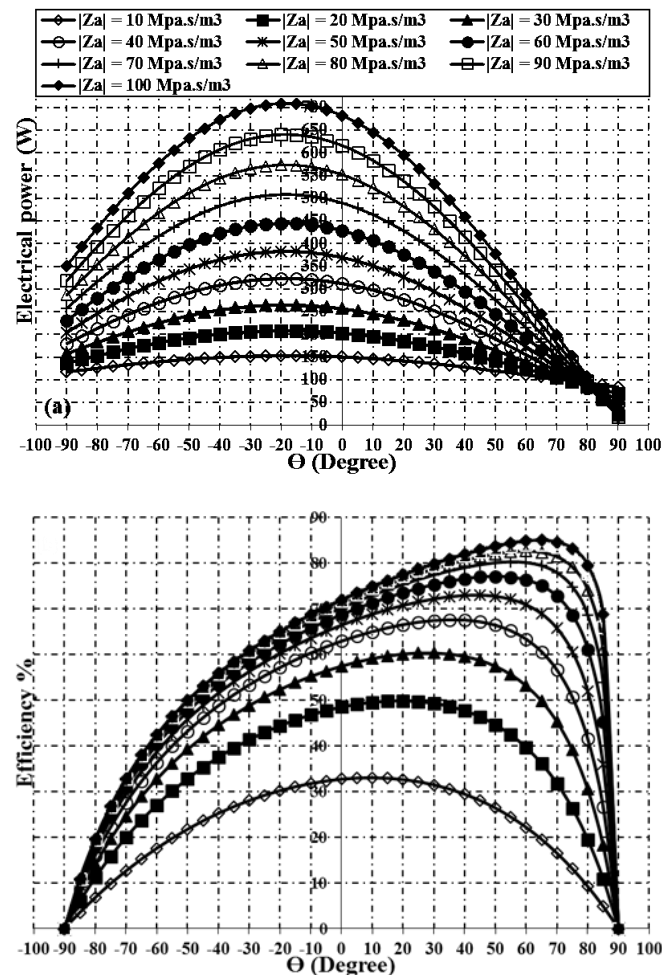

Figure 2. Electrical power consumed (a) and efficiency (electrical power to produced acoustic power) (b) for 1S132M acoustic driver when exposed to different acoustic conditions.
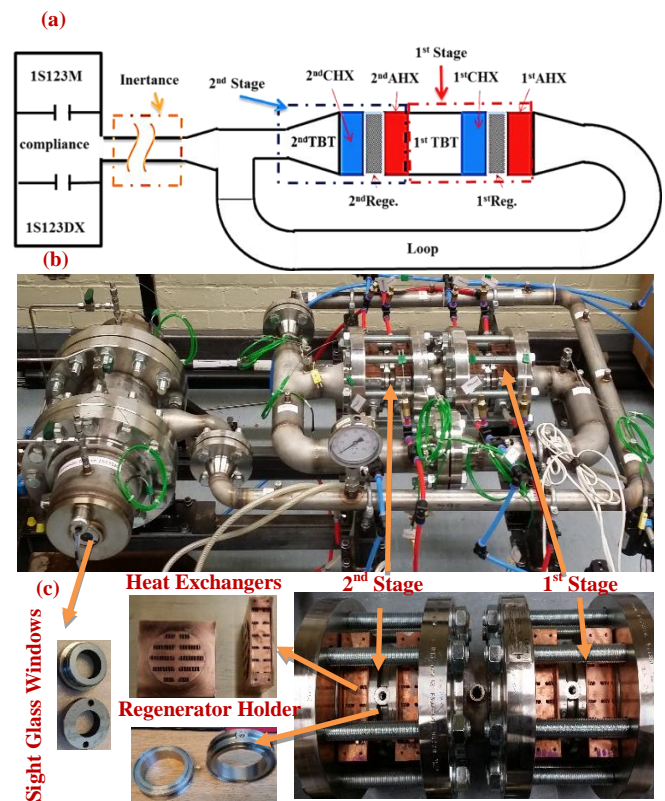

Figure 3. Schematic drawing (a), experimental apparatus (b), heat exchangers, regenerators and glass windows (c).

Table I: Dimensions and details of the optimized design of apparatus.

Component	Length (mm)	Diameter (mm)	Porosity (%)	Hydraulic radius (mm)
Inertance (L)	2850	35	--------	17.5
Torus tube	1445	65	---------	32.5
The first stage/core (1st stage)				
1st AHX	40	100	30	0.5
1st CHX	40	100	30	0.5
1st Reg.	30	100	75	0.03
1st TBT	90	100	------	50
The second stage/core (2nd stage)				
2nd AHX	40	100	30	0.5
2nd CHX	40	100	30	0.5
2nd Reg.	30	100	75	0.03
2nd TBT	90	100 and 65	------	50 and 32.5

The two-stage traveling-wave thermoacoustic cooler has been designed to work at 60 Hz, which is the resonance frequency of the acoustic drivers. The working oscillatory gas is helium at 40 bar. Two function generators (model TG1010A) and one power amplifier with two separate inputs/outputs (model void acoustics - Network 4) have been used to drive the acoustic drivers. The acoustic pressure in front of the moving pistons of the acoustic drivers is measured with a dynamic pressure transducer (PCB Model 106B50), and the displacement of the pistons is measured with a high speed laser displacement sensor (Microtrak II). Two sight glass windows (Metaglas – Type 64) were installed and used to pass the laser through them (see Figure 3c). The pressure and displacement signals acquired simultaneously are converted to signals in the frequency domain by carrying out discrete fast Fourier transform (FFT), to find their relative phase difference. Temperatures at the middle of the ambient and cold heat

exchangers of each stage are measured with K-type thermocouples. Temperatures at the middle and two ends of each regenerator are also measured with K-type thermocouples (see Figure 4).
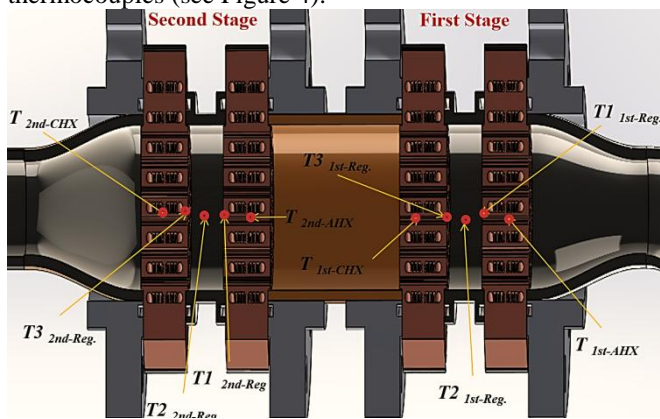

Figure 4. Cross-sectional area shows the temperatures distribution along the two stages of the thermoacoustic refrigerator.

IV. CHARACTERISTICS OF A THERMOACOUSTIC REFRIGERATOR

To build the confidence in the operation of the acoustic drivers and the acoustic field established, the acoustic characteristics of the apparatus were firstly studied by measuring the acoustic pressure amplitude along the thermoacoustic cooler. Its distribution was compared with the results from simulation using DeltaEC. The measured pressure amplitude along the resonator is illustrated by the symbols in Figure. 5. At the operating frequency of 60 Hz, the pressure anti-node of the acoustic field in the apparatus is at the location of the compliance. The distributions of the acoustic pressure amplitude and the volumetric velocity amplitude in the apparatus obtained from simulation are indicated by the solid line in Figure 5., with x = 0 defined as the location of the acoustic drivers (compliance). The difference in pressure between the simulation and the measurement is less than 5 %.

It is established that the phase of velocity is 90° leading the phase of displacement. Hence, the acoustic power delivered by the acoustic drivers, $\dot{E}_{2,A.D}$ could be experimentally evaluated using the following equation:

$$\dot{E}_{2,A.D} = \frac{1}{2}|p_{1,out}||\xi_1|\omega A_{A.D}\cos(\theta_{(p_{1,out\&\xi_1})} - 90°) \quad (4)$$

Where $|p_{1,out}|$ is the amplitude of the acoustic pressure of the fundamental frequency at the front of the acoustic drivers, $\theta_{(p_{1,out\&\xi_1})}$ is the phase difference between the pressure and displacement oscillation. ω is the angular frequency. $A_{A.D}$ and $|\xi_1|$ are the cross-sectional area and the displacement amplitude of the piston of the acoustic drivers, respectively.

The well-known and mostly used two-microphone experimental method have been also utilized to measure the oscillatory pressures and their phases to be then converted to the equivalent acoustic power. This method is based on measuring the pressure amplitude and phase by using pressure transducers at two different positions with a specific distance between them [3].

The performance of a thermoacoustic refrigerator can be evaluated by the cooling coefficient of performance, COP (=

$Q_c/\dot{E}_{2,A.D}$). Q_c is the cooling load. $\dot{E}_{2,A.D}$ is the acoustic power delivered to the system. However, COP only reveals the amount of heat, Q_c, removed from the cold reservoir by doing work $\dot{E}_{2,A.D}$ by the refrigerator. It does not reveal the temperature of the cold reservoir and the temperature difference that the refrigerator has to overcome. The Carnot COP (COPC (= $T_c/(T_a - T_c)$)) is the highest COP that a refrigerator can achieve between two operating temperatures T_c and T_a. T_c and T_a are the temperatures of the cold and ambient/hot reservoir, respectively.

The temperatures measured at the cold and ambient/hot ends of a regenerator are used as T_c and T_a, to exclude the effect of heat transfer efficiency of the heat exchanger. To account for the difference in the performance of a refrigerator operating at different temperatures, the ratio of COP to Carnot COP, COPR, is introduced, which is defined as COPR = COP / COPC.

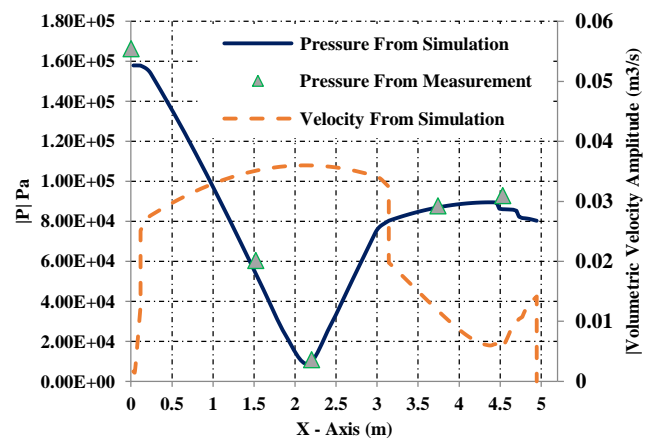
Figure 5. Amplitude of acoustic pressure and velocity along the thermoacoustic cooler.

V. RESULTS AND DISCUSSIONS

The value of the COP of the two-stage traveling-wave thermoacoustic refrigerator is plotted against the different cooling loads/powers (Q_c), as shown in Figure 6. It can be clearly noticed that the dependence of the COP on the cooling load is almost linear due to maintaining the same given acoustic power to the thermoacoustic cooler. A maximum cooling power of about 255W has been achieved with COP of 2.
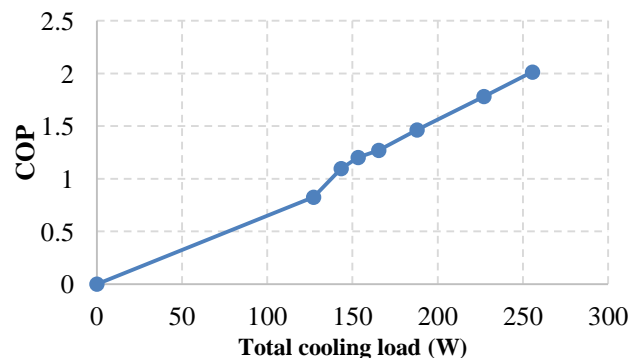

Figure 6. Experimental Performance of thermoacoustic refrigerator (COP) at different cooling loads.

The values of the COPR and difference of temperatures at the ends of the regenerator also have been plotted against the different cooling loads, as shown in Figure 7. This to reveal the temperature difference that the refrigerator can overcome and its performance when operating at different temperatures.
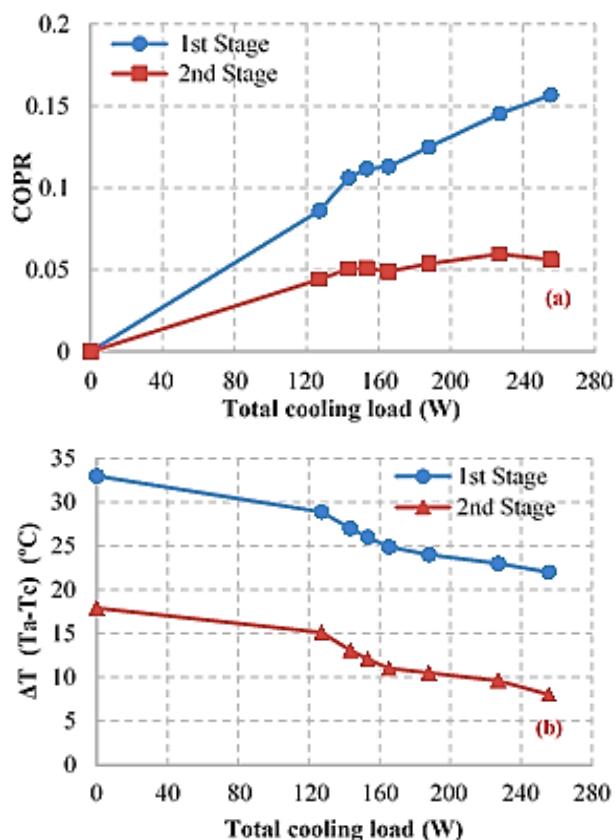
Figure 7. Experimental performance of the thermoacoustic refrigerator, (a) COPR and (b) difference of temperatures at the ends of the regenerator.

The first stage of the thermoacoustic cooler has the capability of achieving 135W of cooling power at COPR of almost 0.16 and difference of temperatures at the ends of the regenerator of 22ºC. The second stage of the thermoacoustic cooler has the capability of achieving 120W of cooling power at COPR of almost 0.056 and difference of temperatures at the ends of the regenerator of only 8ºC.

It can be obviously seen that the performance of the first stage is always higher than the performance of the second stage in terms of the COPR, difference of temperatures at the ends of the regenerator and achieved cooling power. This is due to enabling more acoustic power to firstly pass through the first stage/core and consuming some power to produce the cooling effect, then the left acoustic power will pass through the second stage and that leading to the difference in performances.

The amplitudes of acoustic pressure and acoustic power have been plotted along the apparatus at different cooling loads, with $x = 0$ m defined as the location of the front of the pistons of the acoustic drivers (at the middle of the compliance) and $x = 4.53$m defined as the location of the entrance to the first stage (see Figure 8).

The highest value of the pressure amplitude is at the compliance location where the acoustic drivers, where the minimum value is somewhere close to the middle of the inertance where the velocity is maximum, as shown in Figures 5 and 8a. As it can be noticed from Figure 8b, the acoustic power monotonously vary when different cooling loads applied following the trends of pressure amplitudes. It has been also observed that the values of acoustic power will slightly drop as more cooling loads applied to the thermoacoustic cooler even the delivered acoustic power by the acoustic drivers has been kept almost the same.
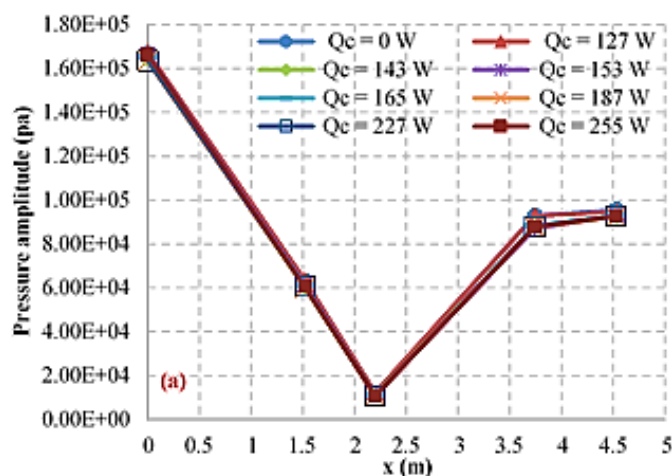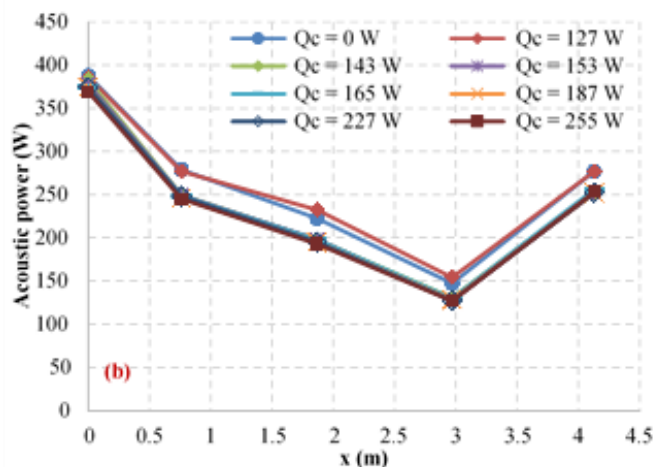

Figure 8. Distribution of the experimentally measured (a) amplitude of acoustic pressure and (b) acoustic power along the thermoacoustic cooler at different cooling load.

Figure 9. shows the experimentally measured temperatures distribution along the two thermoacoustic stages. The cold side of the thermoacoustic refrigerator has reached a minimum temperature of -0.2 and 4.3ºC on the first and second stage respectively. As more cooling load applied to the thermoacoustic cooler these minimum temperatures of the first and second stages will rise to reach 22 and 8 ºC respectively at total cooling power of 255W.

For all cooling load sets, the experimentally measured temperatures along the first regenerator are nonlinearly distributed as the value of the temperature at the center of the first regenerator is close to the hot side temperature rather than being somewhere between the two temperatures of the hot and cold side. This is more likely due to having a thermoacoustic streaming.

The second stage shows similar effect with a slight difference as the temperature at the center of the second regenerator as slightly closer to the hot side temperature than but not as much as the first stage.

Table II: Thermocouples locations

1st thermoacoustic stage		2nd thermoacoustic stage	
x(m)	Thermocouple probe location	x(m)	Thermocouple probe location
4.712	Centre of AHX	4.952	Centre of AHX
4.732	Hot side of the Reg.	4.972	Hot side of the Reg.
4.747	Centre of the Reg.	4.987	Centre of the Reg.
4.762	Cold side of the Reg.	5.002	Cold side of the Reg.
4.782	Centre of CHX	5.022	Centre of CHX

	Thermoacoustic Energy
$\dot{E}_{2,A,D}$	Acoustic power of the acoustic drivers, W
Q_c	Cooling power, W
Reg.	Regenerator
TBT	Thermal buffer tube
δ_k	Thermal penetration depth, m
K	Thermal conductivity, W/m·K
ρ	Density, kg/m^3
c_p	Isobaric specific heat capacity, J/kg·K
ω	Angular frequency, s^{-1}

REFERENCES

[1] Nikolas Rott, 1980. A simple Theory of the Sondhauss Tube. Zurich.
[2] Bisio, G. & Rubatto, G., 1999. Sondhauss and Rijke oscillations- thermodynamic analysis, possible applications and analogies. Energy, 24(2), pp.117–131.
[3] Swift, G. (2001). Thermoacoustic: a unifying perspective for some engines and refrigerators.
[4] Tiwatane, T., & Barve, S. (2014). Thermoacoustic Effect: the Power of Conversion of Sound Energy & Heat Energy: Review, 1(4), 20–28.
[5] Maruyama, N., Iwasaki, Y., Saito, M., Kitaide, Y., & Takiguchi, K. (2014). Principal Characteristics of Thermoacoustic Sound Generator and Refrigerator's Application, (March), 19–21.
[6] Yu, B. et al., 2011. Experimental study of a thermoacoustically-driven traveling wave thermoacoustic refrigerator. Cryogenics, 51(1), pp.49–54.
[7] Luo, E. et al., 2006. Thermoacoustically driven refrigerator with double thermoacoustic-Stirling cycles. Applied Physics Letters, 88(7), p.074102.
[8] Miwa, M. et al., 2006. Measurement of acoustic output power in a traveling wave engine. Ultrasonics, 44 Suppl 1, pp.e1527–9.
[9] Ueda, Y., 2008. Calculation Method for the Prediction of the Performance of a Traveling-Wave Thermoacoustic Cooler. Journal of Power and Energy Systems, 2(5), pp.1276–1282.
[10] Ueda, Y. et al., 2010. Optimization of the regenerator of a traveling-wave thermoacoustic refrigerator. Journal of Applied Physics, 107(3), p.034901.
[11] Bassem, M.M., Ueda, Y. & Akisawa, a., 2011. Design and construction of a traveling wave thermoacoustic refrigerator. International Journal of Refrigeration, 34(4), pp.1125–1131.
[12] Yahya S. G., Mao X. & Jaworski J. A. 2015. Design a Two-Stage Looped-tube Thermoacoustic Cooler for Thermal Management of Enclosures. The 24th IIR International Congress of Refrigeration, 16-22 Aug 2015. Yokohama, Japan: International Institute of Refrigeration.
[13] Wakeland, R. (2000). Use of electrodynamic drivers in thermoacoustic refrigerators. The Journal of the Acoustical Society of America, 107(2), 827–32
[14] Zhang, L. M., Chen, Y. Y., & Luo, E. C. (2014). How to match an acoustical load to a thermoacoustic heat engine, 1445, 1445–1452. doi:10.1063/1.4860877.
[15] Paek, I., Mongeau, L., & Braun, J. E. (2005). A method for estimating the parameters of electrodynamic drivers in thermoacoustic coolers. The Journal of the Acoustical Society of America, 117(1), 185. doi:10.1121/1.1828500.
[16] Backhaus, S. & Swift, G., 2000. A thermoacoustic-Stirling heat engine: detailed study. The Journal of the Acoustical Society of America, 107(6), pp.3148–66.
[17] Luo, E., et al., 2005. A high pressure-ratio, energy- focused thermoacoustic heat engine with a tapered resonator. Chinese Science Bulletin, 50(3), p.284.
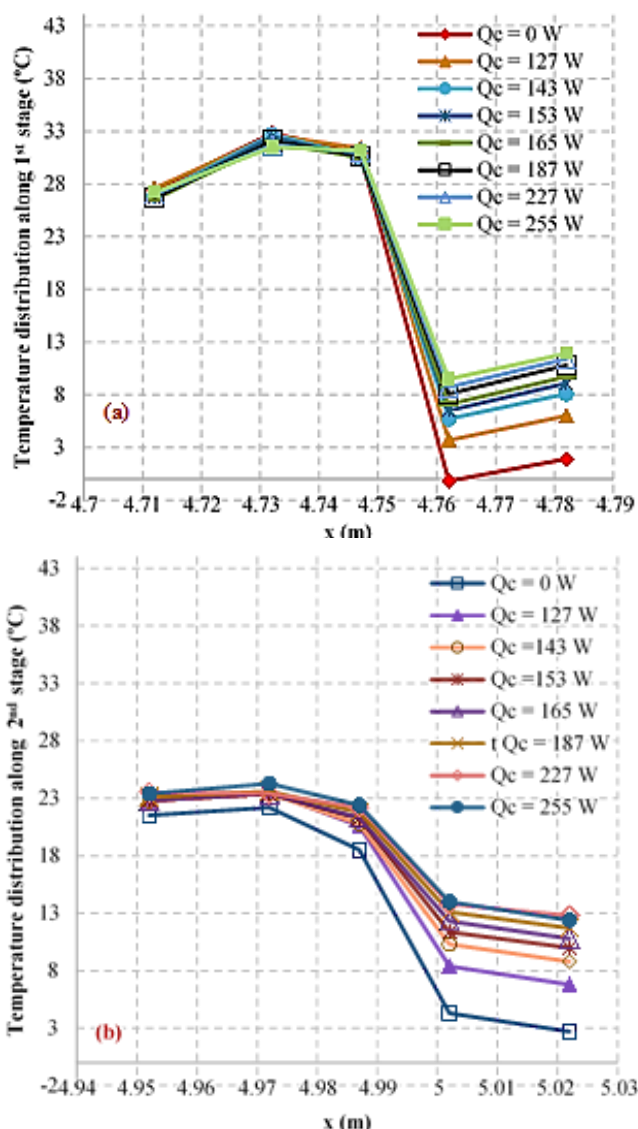
Figure 9. Distribution of the experimentally measured temperatures along the (a) first and (b) second stages of the thermoacoustic cooler at different cooling load.

VI. CONCLUSION AND FUTURE WORK

The performance of acoustic driver (1s132M by Q-Drive) has been analytically studied to deliver the preferable acoustic impedance to work efficiently. The experimental setup and instrumentation of the apparatus of the travelling wave thermoacoustic refrigerator have been presented. The experimental results of the preliminary test obtained from the laboratory prototype have been compared with the numerical DeltaEC modelling. The preliminary tests shows promising results in terms of the cooling power and coefficient of performance (COP). However, a thermoacoustic streaming is more likely present due to the non-linear distribution of temperatures along the regenerator of the first and second stages.

APPENDIX

Table III: List of Symbols and Abbreviations

AHX	Ambient heat exchanger
CHX	Cold heat exchanger
COP	Coefficient of performance
COPR	The ratio of COP to Carnot COP
DeltaEC	Design Environment for Low-amplitude